CLIMATOLOGY

Monsoon-driven Saharan dust variability over the past 240,000 years

C. Skonieczny[1,2]*, D. McGee[2], G. Winckler[3,4], A. Bory[3,5], L. I. Bradtmiller[6], C. W. Kinsley[2], P. J. Polissar[4], R. De Pol-Holz[7], L. Rossignol[8], B. Malaizé[8]

Reconstructions of past Saharan dust deposition in marine sediments provide foundational records of North African climate over time scales of 10^3 to 10^6 years. Previous dust records show primarily glacial-interglacial variability in the Pleistocene, in contrast to other monsoon records showing strong precessional variability. Here, we present the first Saharan dust record spanning multiple glacial cycles obtained using ^{230}Th normalization, an improved method of calculating fluxes. Contrary to previous data, our record from the West African margin demonstrates high correlation with summer insolation and limited glacial-interglacial changes, indicating coherent variability in the African monsoon belt throughout the late Pleistocene. Our results demonstrate that low-latitude Saharan dust emissions do not vary synchronously with high- and mid-latitude dust emissions, and they call into question the use of existing Plio-Pleistocene dust records to investigate links between climate and hominid evolution.

INTRODUCTION

Variations in past mineral dust emissions from the Sahara Desert recorded in marine sediments are central to our understanding of the long-term climatic evolution of North Africa (*1*–*5*). Observational data and modeling experiments indicate that dust emissions are tightly tied to West African monsoon strength, as dust-generating winds and aridity vary in concert on decadal, millennial, and orbital time scales. During wet "Green Sahara" periods, northeasterly winds weaken over the Sahara, while strong northeasterly winds accompany reduced soil moisture and vegetation cover during weak summer monsoon intervals (Supplementary Text) (*6*–*8*). Saharan dust emissions thus vary in opposition to West African monsoon strength, acting as an integrated tracer of regional hydroclimate. In addition to tracing local conditions, windblown dust plays a critical role in Earth's climate system, interacting with incoming and outgoing radiation, affecting cloud formation, and supplying nutrients to the surface ocean and soils (*9*). As the Sahara is the world's largest dust source, records of past Saharan dust deposition offer essential constraints on atmospheric aerosol loads in past climates.

Long-term dust records indicate an increase in mean Saharan dust fluxes over the past 5 million years (Ma), tracing the aridification of North Africa (*3*, *4*). Superimposed on this mean climate change are apparent changes in the time scales of North African climate variability: Dust fluxes vary on precessional [19 and 23 thousand years (ka)] time scales during the Pliocene (5 to 2.6 Ma), consistent with a wide range of monsoon records showing variations in phase with summer insolation (*10*, *11*), and then shift to glacial-interglacial time scales (41 and 100 ka) during the Quaternary (past 2.6 Ma) with limited precessional variability (*4*, *12*). Given the ties between dust emissions and the West African monsoon noted above and in the Supplementary Text, existing dust flux paleorecords thus suggest a strong imprint of changing glacial-interglacial variability on the West African monsoon's evolution over the Quaternary.

This central conclusion of previous work is important to the ongoing debate over the impact of glacial-interglacial changes on monsoon intensity, as some records show evidence for substantial monsoon weakening during glacial periods (*13*–*16*), while others, including some records from Africa, show strong precessional variability and limited response to glacial-interglacial changes (*10*, *17*, *18*). Dust flux records have also been central to investigations of links between climate and hominid evolution, with several studies using the records to identify change points in the mean state and variability of African climate over the past 5 Ma (*4*, *5*, *12*, *19*).

However, questions exist about the fidelity of existing long-term Saharan dust records, which are based either on dust percentages in the sediment or fluxes calculated using age model–based mass accumulation rates (MARs). In the MAR approach, linear sedimentation rates (cm ka^{-1}) are first derived from an age model based on benthic foraminifera $\delta^{18}O$ values and paleomagnetic reversals. Sedimentation rates are then multiplied by dry bulk density measurements (g cm^{-3}) to calculate MARs (g cm^{-2} ka^{-1}) (*3*), and dust MARs are calculated by multiplying higher-resolution dust percent data (noncarbonate sediments) by bulk MARs (Materials and Methods) (*3*). Of these parameters, dust percentages have the greatest role in driving dust MAR variability (Supplementary Materials), and both dust percentages and dust MARs have similar power spectra in long-term Saharan dust records (*4*).

The MAR approach has multiple sources of potential bias (Supplementary Materials). Perhaps most important, because the age-depth relationship is anchored to external age references only at ~20-ka intervals for most sites (*3*), terrigenous fluxes are, in reality, limited to this resolution. Multiplying low-resolution MARs by higher-resolution dust percent data to produce a higher-resolution dust flux record assumes that changes in dust percent are driven solely by changes in dust supply. However, short-term dust percent changes may also be driven by variations in biogenic sediment accumulation in the sediments, for example, due to calcium carbonate dissolution.

These problems can be resolved in late Quaternary sediments by normalizing to the flux of ^{230}Th scavenged from seawater (*20*). This approach allows calculation of high-resolution sediment accumulation

[1]Laboratoire Géosciences Paris-Sud, UMR CNRS 8148, Université de Paris-Sud, Université Paris-Saclay, 91405 Orsay Cedex, France. [2]Department of Earth, Atmospheric and Planetary Sciences, Massachusetts Institute of Technology, Cambridge, MA, USA. [3]Lamont-Doherty Earth Observatory, Columbia University, Palisades, NY, USA. [4]Department of Earth and Environmental Sciences, Columbia University, New York, NY, USA. [5]Université de Lille, CNRS, Université Littoral Cote d'Opale, UMR 8187, LOG, Laboratoire d'Océanologie et de Géosciences, Lille, France. [6]Department of Environmental Studies, Macalester College, St. Paul, MN, USA. [7]GAIA-Antártica, Universidad de Magallanes, Punta Arenas, Chile. [8]Laboratoire Environnements et Paléoenvironnements Océaniques et Continentaux, UMR CNRS 5805, Université de Bordeaux, Pessac, France.
*Corresponding author. Email: charlotte.skonieczny@u-psud.fr

rates that are relatively insensitive to age model errors, lateral sediment redistribution, and carbonate dissolution (Materials and Methods and Supplementary Materials). ^{230}Th normalization has been used to produce high-quality, reproducible records of Saharan dust deposition across the subtropical North Atlantic, but these records are limited to the past 20 ka (*21*–*23*). Here, to clarify the relative role of glacial-interglacial and precessional variations in pacing North African climate changes, we measured ^{230}Th-normalized dust fluxes over the past 240 ka in sediment core MD03-2705 [18°05′N, 21°09′W, 3085 m below sea level (mbsl)] (Fig. 1) (*24*), reaching the effective limit of ^{230}Th normalization at this site. The site is located directly adjacent to Ocean Drilling Program Site 659 (ODP659; Fig. 1), which provides one of the canonical records of Saharan dust emissions over the past 5 Ma (*3*, *4*). These data constitute the first ^{230}Th-normalized Saharan dust flux record spanning multiple glacial-interglacial cycles.

RESULTS

Throughout the past 240 ka, ^{230}Th-normalized dust fluxes at MD03-2705 present recurring fluctuations between minima around 0.5 g cm^{-2} ka^{-1} and maxima reaching ~1.5 to 1.75 g cm^{-2} ka^{-1}, with one extreme reaching 2.5 g cm^{-2} ka^{-1} (Fig. 2 and table S2). The time history of dust fluxes parallels summer insolation at 65°N, with dust minima consistently occurring during insolation maxima (Fig. 2). We compare MD03-2705 dust percentages, which are the dominant drivers of orbital variability in age model–based MARs (Supplementary Materials; figs. S2 and S3), against our ^{230}Th-normalized dust fluxes (Fig. 2). The two records show similar variability for most of the past 240 ka, but important differences emerge between 160 to 140 ka, 70 to 60 ka, and 25 to 20 ka, corresponding to the peaks of the Marine Isotope Stage (MIS) 6, 4, and 2 glacial stages, respectively (Fig. 2). In each case, dust percentages indicate high dust deposition, while ^{230}Th normalization indicates moderate dust fluxes (Fig. 2).

We interpret these differences as reflecting the impact of carbonate dissolution on dust percentages and thus age model–based MARs. As indicated by the carbon and oxygen isotopic ratios measured on MD03-2705 benthic foraminifera ($\delta^{13}C_{ben}$ and $\delta^{18}O_{ben}$, respectively) (*25*), these three periods correspond to periods when $\delta^{13}C_{ben}$ is depleted and $\delta^{18}O_{ben}$ is enriched (Fig. 2). These isotopic changes have been interpreted as representing deep ocean circulation changes that bring corrosive southern-sourced deep water to the site (*25*), leading to increased dissolution of the calcium carbonate deposited at the site. Reconstructions in the low- and mid-latitude North Atlantic indicate decreases in carbonate ion concentrations at similar depths (3.3 to 3.6 km) during MIS 2, 4, and 6 (*26*, *27*), consistent with increased carbonate dissolution at our core site at these times. This hypothesis is supported by decreases in ^{230}Th-normalized $CaCO_3$ burial fluxes during these episodes (Fig. 2, Supplementary Text, and fig. S5). As a result of carbonate dissolution, dust percentages in the sediment rise during glacial periods independent of changes in eolian supply. ^{230}Th-normalized fluxes measured at high resolution identify that these periods are marked by lower carbonate and total sediment fluxes (Fig. 2), but the drop in total sediment flux is missed by the age model–based approach (fig. S2) due to its low-resolution MAR estimates, leading to an overestimate of dust fluxes during glacial maxima.

Spectral analyses were conducted on the MD03-2705 and ODP659 dust percentages (Fig. 3) and dust MARs (Supplementary Materials and fig. S3) for the past 240 ka. As noted previously for the past 2.6 Ma (*4*), ODP659 dust percentage variance over the past 240 ka (Fig. 3) is concentrated at 100- and 41-ka cyclicities, the same time scales of variability in global ice volume and atmospheric CO_2 levels. While the length of the studied period (240 ka) is too short to make firm conclusions about 100-ka cyclicity, the 41-ka variability is robust. The spectrum for MD03-2705 dust percentages is similar (Fig. 3). The precessional 19- and 23-ka cyclicities show lower variance in these spectra, consistent with previous studies on ODP659 that have suggested dominant glacial-interglacial pacing of North African climate change (Fig. 3) (*4*). The similarities of the cores' spectra with each other and with spectra calculated over the past 2.6 Ma in ODP659 confirm that the two sites register the same regional eolian history and that the past 240 ka is representative of the balance between

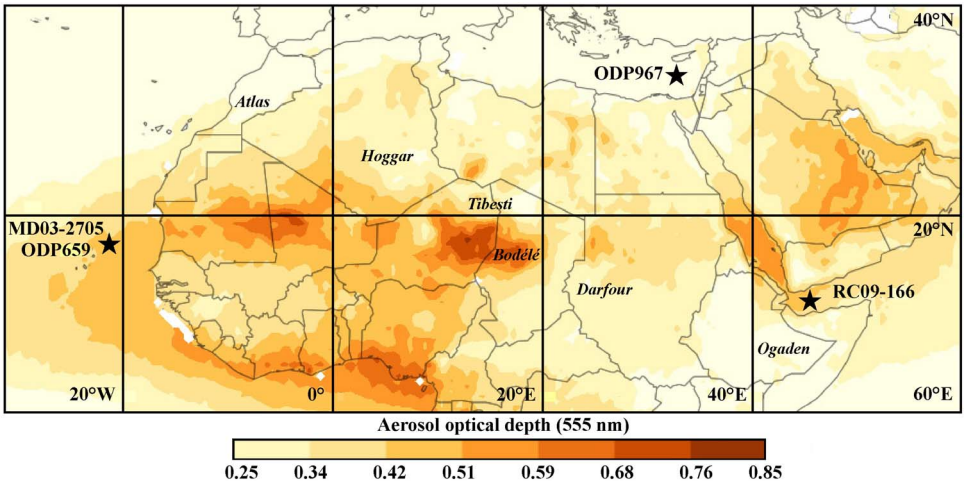

Fig. 1. Modern dust over North Africa and core sites discussed in the text. Map of mean annual (2000–2017) dust aerosol optical depth (AOD) over the North African continent, the northeastern Atlantic Ocean, the Mediterranean Sea, and the Gulf of Aden (off East Africa). Dust AOD data are from the 555-nm nonspherical AOD retrieval averaged between 2000 and 2017 from the Multiangle Imaging Spectroradiometer (source: Giovanni, NASA EarthData). Cores discussed in the manuscript are plotted: sites MD03-2705 (this study) and ODP659 (*3*) in the northeast Atlantic, site ODP967 in the eastern Mediterranean Sea (*28*), and core RC09-166 in the Gulf of Aden (*17*). MD03-2705 and ODP659 are located under the present-day dust plumes transporting Saharan dust across the Atlantic Ocean.

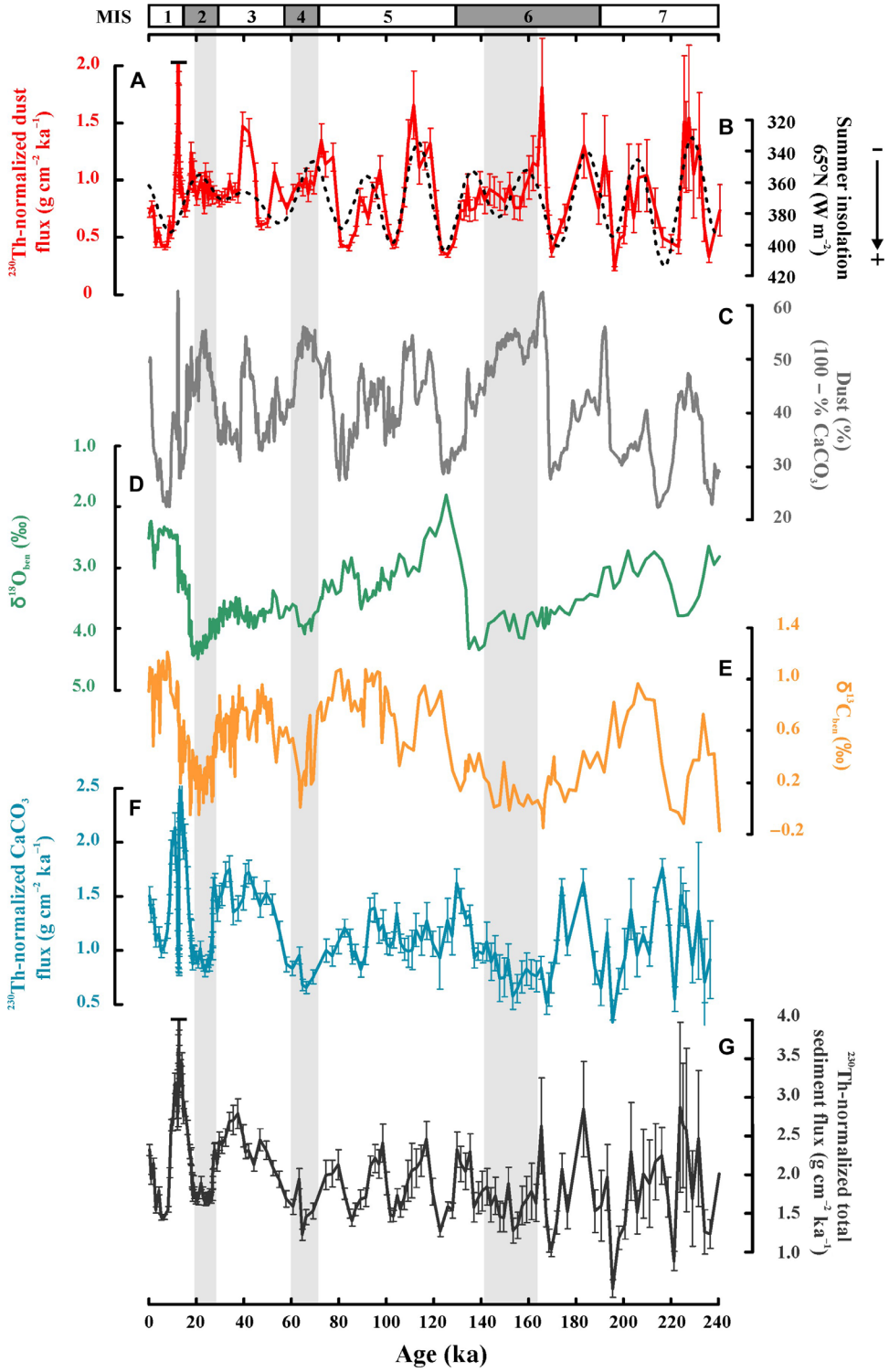

Fig. 2. Dust and paleoceanographic records from core MD03-2705 off West Africa. (**A**) ^{230}Th-normalized dust fluxes (red). (**B**) Northern Hemisphere summer insolation (June-July-August, 65°N; dashed lines) (*29*). (**C**) Dust percentages (gray). (**D** and **E**) $\delta^{18}O_{ben}$ (green) and $\delta^{13}C_{ben}$ (orange) values from benthic foraminifera (*25*). (**F** and **G**) ^{230}Th-normalized $CaCO_3$ flux (blue) and total sediment flux (black). All uncertainties are 1-σ. Gray bars highlight periods when high dust percentages occur in association with low ^{230}Th-normalized sedimentation rates and carbonate accumulation rates, indicating that these dust percentage maxima are driven by carbonate dissolution rather than eolian supply.

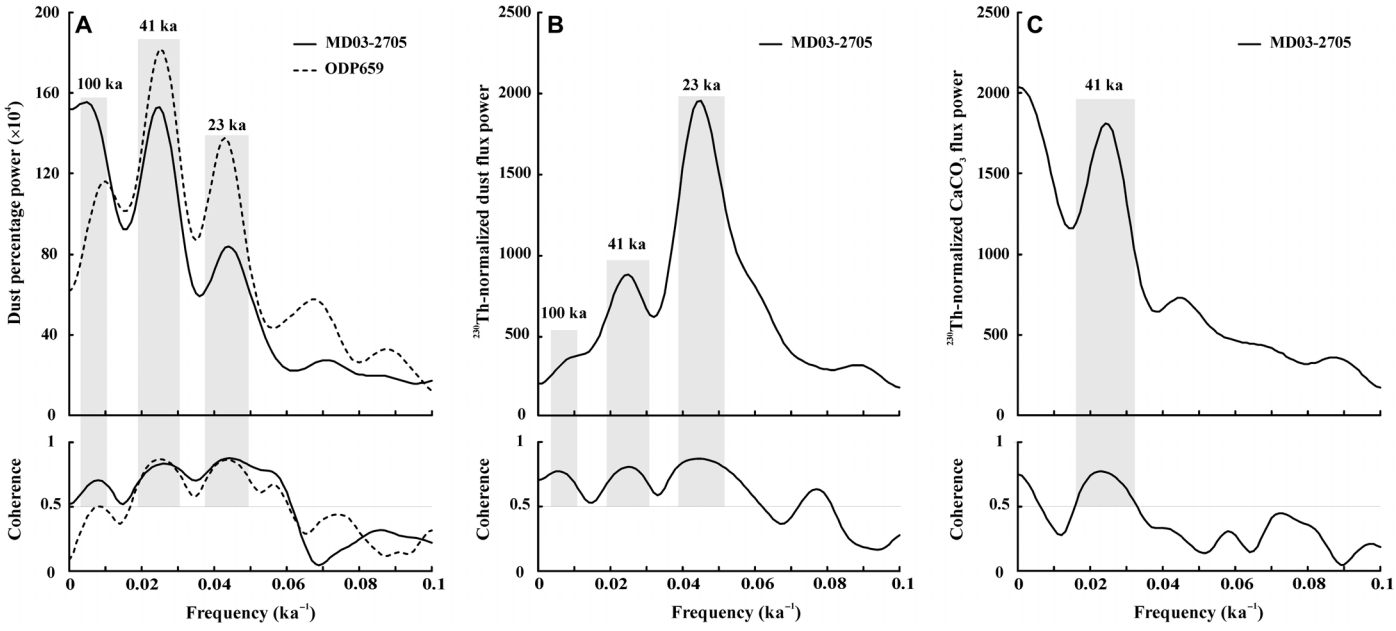

Fig. 3. Power spectral analysis of Saharan dust and carbonate records. Power spectral analyses (top) and associated coherences (bottom) conducted with the AnalySeries software (*46*). (**A**) ODP659 and MD03-2705 dust percentages, (**B**) MD03-2705 ^{230}Th-normalized dust fluxes, and (**C**) MD03-2705 ^{230}Th-normalized carbonate fluxes for the past 240 ka. Dashed line represents ODP659 data, and black line represents MD03-2705 data. Gray bars highlight the main orbital cyclicities (100, 41, and 23 ka) for which a peak in power variance is associated with a coherence higher than 0.5. While the length of the studied period (240 ka) is too short to make firm conclusions about 100-ka cyclicity, the changes in 41- and 23-ka variabilities are robust.

high- and low-latitude impacts on Saharan dust fluxes during the late Pleistocene.

The ^{230}Th-normalized dust fluxes produce a very different spectrum of variability over the past 240 ka (Fig. 3). Our record shows a clear dominance of precessional forcing relative to 41- and 100-ka periodicities, in sharp contrast to the spectra of the dust percentage. While longer records will be necessary to further test the change in 100-ka cyclicity, the shift away from 41-ka variability toward precessional time scales is robust (Supplementary Materials and fig. S4). Further, both the last two glacial maxima show high dust percentages, while ^{230}Th-normalized dust fluxes are only similar to Late Holocene dust fluxes (Fig. 2). The apparent dominance of glacial-interglacial variability on Saharan dust records in previous studies appears to be an artifact of the methods used to estimate fluxes, as carbonate dissolution caused by glacial-interglacial changes in ocean circulation led to overestimation of dust percentages and thus dust MARs during glacial maxima. This hypothesis is supported by spectral analysis of ^{230}Th-normalized $CaCO_3$ fluxes, which indicates the predominance of 41-ka cyclicity (Fig. 3). Our data suggest that, at least during the last two glacial-interglacial cycles, Saharan dust fluxes off West Africa were primarily driven by precessional variations in summer insolation.

DISCUSSION

This finding is consistent with a wide range of other monsoon proxies from North and East Africa that show high-amplitude precessional variability (Fig. 4). Sapropels in the eastern Mediterranean (Fig. 1), a marker of high Nile River discharge, occur during each of the dust flux minima in our record over the past 240 ka and show clear precessional pacing (Fig. 4) (*28*). Similarly, δD values in leaf waxes from the Gulf of Aden (Fig. 1), a tracer of monsoon intensity in East Africa (*17*), show strong similarities with our record (Fig. 4). Records of the accumulation of windblown freshwater diatoms in Tropical Atlantic sediments, a tracer of the desiccation of Saharan lakes at the end of wet periods, also show precessional variability with little power at 41- and 100-ka periods (*18*).

Many of these records also agree in showing "skipped beats" of monsoon intensity during glacial periods (Fig. 4), when there appears to be muted variability in regional aridity despite fluctuating local summer insolation. This observation is consistent with modulation of the response to summer insolation changes by eccentricity and obliquity, as reflected in the combined ETP curve (Fig. 4) (*29*); in both MIS3 and MIS6, precessional maxima in local summer insolation occur during times of low eccentricity and obliquity, leading to reduced heating of high-latitude Northern Hemisphere land masses, potentially muting the monsoon response. Alternatively, it may be that glacial boundary conditions (low CO_2, greater ice volume) raise the threshold for monsoon responses to summer insolation changes. Regardless, the convergence between these records indicates coherent changes in monsoon intensity in both East and West Africa recorded in a wide range of proxy types on precessional time scales (Fig. 4).

However, the relative importance of glacial-interglacial versus precessional variations in "monsoon" records may vary across the continent and between proxies. For example, while the Gulf of Aden δD_{wax} record shows a precessional signal (Fig. 4) (*17*), the spectral analysis of this record also indicates a strong imprint of glacial-interglacial changes (fig. S6). Comparable differences are evident in other monsoon regions as well: In the East Asian summer monsoon region, speleothem $\delta^{18}O$ records show primarily precessional variability (*10*), while precipitation records from Chinese loess (*14*), a reconstruction of Yellow River discharge (*16*), and other records [e.g., (*30*)] show a stronger role for glacial-interglacial variability. On a global scale, records of

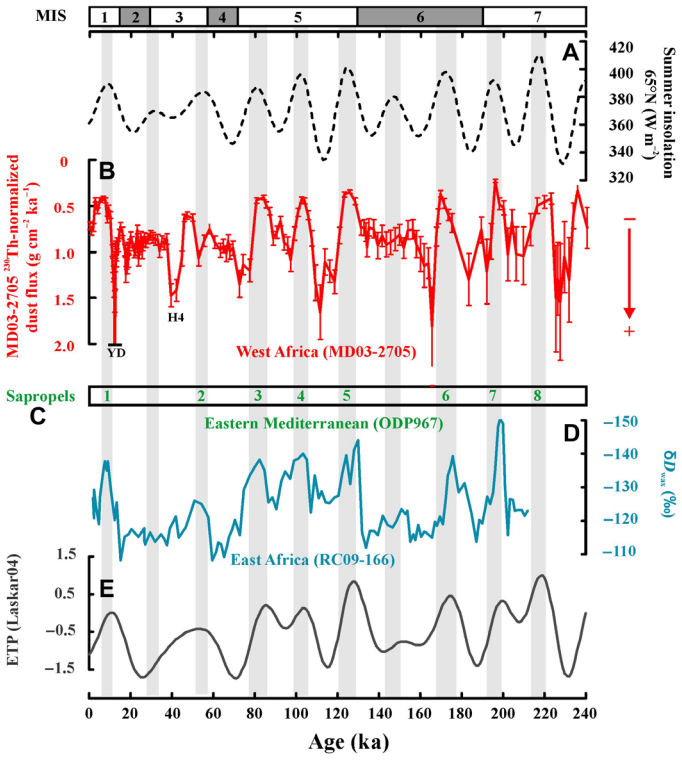

Fig. 4. African monsoon belt records and orbital forcing. (**A**) Northern Hemisphere summer insolation (65°N; dashed lines). (**B**) ^{230}Th-normalized Saharan dust fluxes from core MD03-2705 (red; reversed scale). (**C**) Sapropel numbers from ODP967 in the eastern Mediterranean Sea, reflecting peaks in Nile River runoff (*28*). (**D**) δ*D* values in leaf waxes from core RC09-166 in the Gulf of Aden (blue) (*17*). (**E**) Eccentricity-tilt-precession (ETP) parameter (gray) (*29*). Gray bars highlight maxima of 65°N summer insolation, demonstrating consistent monsoon responses to most insolation maxima and skipped beats during glacial maxima.

the isotopic composition of atmospheric oxygen are dominated by precessional variability (*31*, *32*), providing support for a primary role of summer insolation in modulating globally averaged tropical rainfall over land. These differences highlight the need for future work to systematically examine the relative importance of precessional and glacial-interglacial forcings for different proxies and regions. This study's contribution to these efforts is to demonstrate that apparent glacial-interglacial variation in the previous dust flux records off West Africa was an artifact of the methodology; more broadly, our work suggests the importance of considering other aspects of glacial-interglacial changes that may create apparent 100- and 41-ka variability in proxy records interpreted as reflecting monsoon intensity or rainfall amount.

Although glacial-interglacial variability does not appear to have strong effects on dust emissions from North Africa, high-latitude climate does affect monsoon strength during millennial-scale North Atlantic cooling events (stadials). In particular, the MD03-2705 record shows a millennial-scale peak in dust fluxes during the most recent stadial, the Younger Dryas (12.7 to 11.9 ka; Fig. 4), consistent with dust records spanning the deglaciation (*21*, *22*, *24*, *33*, *34*). Prior to 25 ka, the lower sampling resolution (~2 ka) limits our ability to identify millennial-scale variability, but the dust flux peak at ~40 ka may correspond to Heinrich stadial 4 (Fig. 4).

This study provides a new and clearer picture of late Pleistocene North African climate variability, with implications for our understanding both of African climate evolution and of glacial-interglacial dust variability. First, our data demonstrate that the primary driver of North African climate on multimillennial time scales is Northern Hemisphere summer insolation rather than glacial-interglacial variability. Given the dominance of precession even in the past 240 ka, when the amplitude of glacial-interglacial variability has been near its maximum for the past 5 Ma, this finding suggests that North African climate evolution is unlikely to bear a strong imprint of changes in the amplitude and timing of glacial-interglacial cycles over the Plio-Pleistocene. The overall increase in glacial intensity and duration over the Pleistocene is likely to have increased the number and magnitude of millennial-scale drying events in North Africa associated with North Atlantic stadials and may have created more skipped precessional beats as observed in records of the last two glacial maxima (Fig. 4). However, it appears less likely that these changes in glacial-interglacial cycles are a dominant pacemaker of North African climate. Specifically, our results call into question the use of existing long-term dust records for investigations of changes in North African climate variability and its potential links to hominid evolution (*4*, *5*, *12*, *19*), as these records overstate the importance of glacial-interglacial changes due to biases related to carbonate dissolution.

Second, our findings demonstrate for the first time that Saharan dust fluxes do not vary synchronously with dust fluxes from high- and mid-latitude sources on glacial-interglacial time scales. While emissions from high- and mid-latitude sources increase by a factor of 2 to 4 during glacial periods (*35*–*37*) and thus may play a significant role in amplifying glacial-interglacial cycles through impacts on radiation or carbon storage in the ocean, low-latitude Saharan dust does not show significant glacial-interglacial variability. As the Sahara is the world's strongest source of dust to the atmosphere, our findings have important implications for efforts to estimate dust loads during glacial periods and to model the role of dust in glacial-interglacial transitions. Rather than tracking glacial-interglacial changes, dust fluxes from the Sahara primarily reflect the imprint of precessional variability in local summer insolation, demonstrating coherent variability in the African monsoon belt throughout the late Pleistocene.

MATERIALS AND METHODS

Core sites

Sites ODP659 (18°04.63′N, 21°01.57′W, 3070 mbsl) and MD03-2705 (18°05.81′N, 21°09.19′W, 3085 mbsl) (Fig. 1) were drilled on a seamount off the Mauritanian coast, West Africa (*3*, *25*). This seamount culminates 300 m above the submarine ridge, connecting the Cape Verde Archipelago to the African margin (*24*). Relatively distant from the continent (~500 km) and from potential fluvial sediment sources (*38*, *39*), as well as far from the main turbidite and contourite deposition zones (*40*), this oceanic area is located under the present-day seasonal Saharan dust plumes (Fig. 1) (*41*). Considering this setting, it is assumed that the inorganic fraction recorded at these sites is dominantly from eolian origin.

^{230}Th normalization

^{230}Th normalization is used to calculate sedimentary accumulation rates for MD03-2705. The method relies on the fact that ^{230}Th is produced at a known rate from the decay of dissolved ^{234}U in seawater. As U is a conservative ion in seawater, with a residence time of ~400 ka (*42*), its concentration and isotopic composition are unlikely to have varied substantially over the past 240 ka. Thorium is highly insoluble

("particle reactive") in seawater, and therefore, ^{230}Th quickly adsorbs to falling particles after it is produced and has a residence time of only a few decades (*42*). ^{230}Th fluxes to the seafloor over multidecadal and longer time scales are thus approximately equal to ^{230}Th production in the water column and are largely independent of sediment fluxes (*20*, *43*). It then follows that bulk sediment fluxes are inversely proportional to concentrations of unsupported, decay-corrected ^{230}Th ($^{230}Th_{xs,0}$)

$$F = \frac{\beta \cdot z}{\left(^{230}Th_{xs,0}\right)} \quad (1)$$

where F is the bulk sediment flux (g m^{-2} year^{-1}), β is the ^{230}Th water column production rate from the decay of ^{234}U (0.0267 dpm m^{-3} year^{-1}), z is the water column depth (m), and ($^{230}Th_{xs,0}$) is ^{230}Th activity (dpm g^{-1}) corrected for ^{230}Th associated with detrital sediments, ^{230}Th ingrown from authigenic uranium precipitated in the sediments, and ^{230}Th decay since the deposition of the sediment. A ^{238}U/^{232}Th activity ratio of 0.5 ± 0.1 (1-σ) was used to estimate ^{230}Th associated with detrital material and authigenic U. For a detailed discussion of these corrections, see (*20*). Uncertainties associated with these corrections increase both with age and with the detrital content of the samples, making ~240 ka the effective upper limit for ^{230}Th normalization in these sediments.

U-Th data for the past 26 ka were analyzed at the University of British Columbia and were published in (*44*). The samples for this study were prepared and analyzed at the Massachusetts Institute of Technology (MIT) using standard techniques (*23*, *45*). Samples weighing ~50 mg each were spiked with ^{236}U and ^{229}Th solutions and dissolved in Savillex PFA vials with nitric, hydrochloric, and hydrofluoric acids as well as hydrogen peroxide. Following conversion to hydrochloric acid and addition of iron in solution, ammonium hydroxide was added to neutralize the samples and precipitate iron oxyhydroxides, scavenging U and Th and leaving behind soluble ions. These ions were removed by centrifugation. The iron oxyhydroxides were then redissolved in nitric acid, and U and Th were isolated using 2-ml anion exchange columns containing AG1-X8 100- to 200-mesh resin.

U and Th fractions were analyzed separately in static mode using a Nu Plasma II-ES multiple collector inductively coupled plasma mass spectrometer equipped with a glass spray chamber, with a sensitivity in wet plasma mode of ~40 V/ppm (parts per million) for U and Th. ^{230}Th and ^{234}U were analyzed using an ion counter, while all other isotopes were measured using Faraday cups. Ion counter gain was evaluated every five samples using CRM-112a (50 ng/g) for U and an in-house ^{229}Th-^{230}Th-^{232}Th standard (MITh-1) for Th. Dynamic measurements of 230.5 and 229.5 were performed on each sample using the ion counter to assess tailing of ^{232}Th on ^{230}Th. Procedural blanks were included with each set of chemistry and were negligible (<0.5%). Total uncertainties from mass spectrometry after inclusion of uncertainties for counting statistics, mass bias corrections, ion counter gain, tailing, and procedural blank were <1% for all isotope ratios, much smaller than uncertainties associated with estimating $^{230}Th_{xs}$ concentrations from isotope data.

Calcium carbonate content

$CaCO_3$ percentages for each sample were measured at Macalester College by coulometry, following methods in (*7*). Although eolian dust may contain detrital calcium carbonate, calcium carbonate contents at MD03-2705 are dominantly of marine biogenic origin, mainly foraminifera and coccoliths (*25*).

Cross-spectral analysis

To interrogate the different dust records for Milankovitch periodicities in the frequency (spectral) domain, we used the AnalySeries software package (*46*). The data have been processed by spectral analysis to examine the response of the dust records in the main frequency bands of orbital forcing, ~1/23 ka^{-1} and 1/19 ka^{-1} (precession), 1/41 ka^{-1} (obliquity), and ice-volume variations (about 1/100 ka^{-1}). We used the Blackman-Tukey method of cross-spectral analysis with a Bartlett-type window, providing an 80% confidence interval (*47*–*49*) to identify periods where significant variance is concentrated. Spectra and coherence of dust records were calculated against ETP (*29*) over the past 240 ka to assess the extent to which local and ETP signals are linearly correlated in each frequency band. Results of the spectral analysis are presented as variance power. When similar periodicities are present in any two signals (dust record and ETP), cross-spectral analysis is used to define the level of coherence at these periods (*49*). Coherence is a measure of the degree to which two signals are linearly related to a zero-base correlation coefficient and is considered significant (at the 80% level) if larger than 0.5. Because of the fact that sedimentation rate and sampling resolution are not constant, the time spacing between the samples is not regular. To obtain a regular time sampling, all data were linearly interpolated and resampled on the basis of the ETP curve resolution (*29*). The spectral analysis was performed on the past 240 ka time periods, and the studied frequencies range from 0 to 0.1 ka^{-1}. We note that the temporal window considered in the present work (past 240 ka) is relatively short for reliable results in the 100-ka frequency range.

SUPPLEMENTARY MATERIALS

Supplementary material for this article is available at http://advances.sciencemag.org/cgi/content/full/5/1/eaav1887/DC1

Supplementary Material and Methods

Supplementary Text

Fig. S1. MD03-2705 age model for the past 240 ka.

Fig. S2. Sedimentological parameters used in the dust MAR calculation for MD03-2705 and ODP659 for the past 240 ka.

Fig. S3. Power spectral analysis of MD03-2705 and ODP659 dust MARs.

Fig. S4. Power spectral analysis of MD03-2705 ^{230}Th-normalized dust flux records at the extremes of 1-σ uncertainties.

Fig. S5. Comparison between MD03-2705 ^{230}Th-normalized $CaCO_3$ fluxes and reconstructed [CO_3^{2-}] from *Cibicidoides wuellerstorfi* B/Ca between 90 and 50 ka.

Fig. S6. Power spectral analysis of RC09-166 δD_{wax} (East Africa).

Table S1. Age control points used to build the chronology of the past 240 ka of core MD03-2705.

Table S2. MD03-2705 core depth, model age, thorium and uranium activities, and carbonate content as well as sediment, dust, and carbonate fluxes for the past 240 ka.

References (*50*–*73*)

REFERENCES AND NOTES

1. M. Sarnthein, G. Tetzlaff, B. Koopmann, K. Wolter, U. Pflaumann, Glacial and interglacial wind regimes over the eastern subtropical Atlantic and North-West Africa. *Nature* **293**, 193–196 (1981).
2. D. K. Rea, The paleoclimatic record provided by eolian deposition in the deep sea: The geologic history of wind. *Rev. Geophys.* **32**, 159–195 (1994).
3. R. Tiedemann, M. Sarnthein, N. J. Shackleton, Astronomic timescale for the Pliocene Atlantic d^{18}O and dust flux records of Ocean Drilling Program Site 659. *Paleoceanography* **9**, 619–638 (1994).
4. P. B. deMenocal, Plio-Pleistocene African climate. *Science* **270**, 53–59 (1995).
5. P. B. deMenocal, African climate change and faunal evolution during the Pliocene–Pleistocene. *Earth Planet. Sci. Lett.* **220**, 3–24 (2004).
6. W. Wang, A. Evan, C. Flamant, C. Lavaysse, On the decadal scale correlation between African dust and sahel rainfall: The role of Saharan heat low–forced winds. *Sci. Adv.* **1**, e1500646 (2015).

7. L. I. Bradtmiller, D. McGee, M. Awalt, J. Evers, H. Yerxa, C. W. Kinsley, P. B. deMenocal, Changes in biological productivity along the northwest African margin over the past 20,000 years. *Paleoceanography* **31**, 185–202 (2016).
8. S. Egerer, M. Claussen, C. Reick, Rapid increase in simulated North Atlantic dust deposition due to fast change of northwest African landscape during the Holocene. *Clim. Past* **14**, 1051–1066 (2018).
9. D. R. Muhs, The geologic records of dust in the Quaternary. *Aeolian Res.* **9**, 3–48 (2013).
10. H. Cheng, R. L. Edwards, A. Sinha, C. Spötl, L. Yi, S. Chen, M. Kelly, G. Kathayat, X. Wang, X. Li, X. Kong, Y. Wang, Y. Ning, H. Zhang, The Asian monsoon over the past 640,000 years and ice age terminations. *Nature* **534**, 640–646 (2016).
11. C. Rose, P. J. Polissar, J. E. Tierney, T. Filley, P. B. deMenocal, Changes in northeast African hydrology and vegetation associated with Pliocene–Pleistocene sapropel cycles. *Philos. Trans. R. Soc. B* **371**, 20150243 (2016).
12. M. H. Trauth, J. C. Larrasoaña, M. Mudelsee, Trends, rhythms and events in Plio-Pleistocene African climate. *Quat. Sci. Rev.* **28**, 399–411 (2009).
13. A. Tisserand, B. Malaizé, E. Jullien, S. Zaragosi, K. Charlier, F. Grousset, African monsoon enhancement during the penultimate glacial period (MIS 6.5 ~ 170 ka) and its atmospheric impact. *Paleoceanography.* **24**, PA2220 (2009).
14. J. W. Beck, W. Zhou, C. Li, Z. Wu, L. White, F. Xian, X. Kong, Z. An, A 550,000-year record of East Asian monsoon rainfall from ^{10}Be in loess. *Science* **360**, 877–881 (2018).
15. Y. Cai, I. Y. Fung, R. L. Edwards, Z. An, H. Cheng, J. E. Lee, L. Tan, C.-C. Shen, X. Wang, J. A. Day, W. Zhou, M. J. Kelly, J. C. H. Chiang, Variability of stalagmite-inferred Indian monsoon precipitation over the past 252,000 y. *Proc. Natl. Acad. Sci. U.S.A.* **112**, 2954–2959 (2015).
16. S. C. Clemens, A. Holbourn, Y. Kubota, K. E. Lee, Z. Liu, G. Chen, A. Nelson, B. Fox-Kemper, Precession-band variance missing from East Asian monsoon runoff. *Nat. Commun.* **9**, 3364 (2018).
17. J. E. Tierney, P. B. deMenocal, P. D. Zander, A climatic context for the out-of-Africa migration. *Geology* 1023–1026 (2017).
18. E. M. Pokras, A. C. Mix, Earth's precession cycle and Quaternary climatic change in tropical Africa. *Nature* **326**, 486–487 (1987).
19. J. F. Donges, R. V. Donner, M. H. Trauth, N. Marwan, H.-J. Schellnhuber, J. Kurths, Nonlinear detection of paleoclimate-variability transitions possibly related to human evolution. *Proc. Natl. Acad. Sci. U.S.A.* **108**, 20422–20427 (2011).
20. R. Francois, M. Frank, M. M. Rutgers van der Loeff, M. P. Bacon, ^{230}Th normalization: An essential tool for interpreting sedimentary fluxes during the late Quaternary. *Paleoceanography* **19**, PA1018 (2004).
21. J. Adkins, P. deMenocal, G. Eshel, The "African humid period" and the record of marine upwelling from excess ^{230}Th in Ocean Drilling Program Hole 658C. *Paleoceanography* **21**, 1–14 (2006).
22. D. McGee, P. B. deMenocal, G. Winckler, J. B. W. Stuut, L. I. Bradtmiller, The magnitude, timing and abruptness of changes in North African dust deposition over the last 20,000 yr. *Earth Planet. Sci. Lett.* **371–372**, 163–176 (2013).
23. R. H. Williams, D. McGee, C. W. Kinsley, D. A. Ridley, S. Hu, A. Fedorov, I. Tal, R. W. Murray, P. B. deMenocal, Glacial to Holocene changes in trans-Atlantic Saharan dust transport and dust-climate feedbacks. *Sci. Adv.* **2**, e1600445 (2016).
24. E. Jullien, F. Grousset, B. Malaizé, J. Duprat, M. F. Sanchez-Goni, F. Eynaud, K. Charlier, R. Schneider, A. Bory, V. Bout, J. A. Flores, Low-latitude "dusty events" vs. high-latitude "icy Heinrich events." *Quat. Res.* **68**, 379–386 (2007).
25. B. Malaizé, E. Jullien, A. Tisserand, C. Skonieczny, E. F. Grousset, F. Eynaud, C. Kissel, J. Bonnin, S. Karstens, P. Martinez, A. Bory, V. Bout-Roumazeilles, T. Caley, X. Crosta, K. Charlier, L. Rossignol, J.-A. Abel, R. Schneider, The impact of African aridity on the isotopic signature of Atlantic deep waters across the Middle Pleistocene Transition. *Quat. Res.* **77**, 182–191 (2012).
26. W. S. Broecker, J. Yu, A. E. Putnam, Two contributors to the glacial CO_2 decline. *Earth Planet. Sci. Lett.* **429**, 191–196 (2015).
27. J. Yu, L. Menviel, Z. D. Jin, D. J. R. Thornalley, S. Barker, G. Marino, E. J. Rohling, Y. Cai, F. Zhang, X. Wang, Y. Dai, P. Chen, W. S. Broecker, Sequestration of carbon in the deep Atlantic during the last glaciation. *Nat. Geosci.* **9**, 319–324 (2016).
28. D. Kroon, I. Alexander, M. Little, L. J. Lourens, A. Matthewson, A. H. F. Robertson, T. Sakamoto, Oxygen isotope and sapropel stratigraphy in the eastern Mediterranean during the last 3.2 million years, in *Proceedings of the Ocean Drilling Program, Scientific Results*, A. H. F. Robertson, K.-C. Emeis, C. Richter, A. Camerlenghi, Eds. (Ocean Drilling Program, 1998), vol. 160, pp. 181–189.
29. J. Laskar, P. Robutel, F. Joutel, M. Gastineau, A. C. M. Correia, B. Levrard, A long-term numerical solution for the insolation quantities of the Earth. *Astron. Astrophys.* **428**, 261–285 (2004).
30. Y. Sun, J. Kutzbach, Z. An, S. Clemens, Z. Liu, W. Liu, X. Liu, Z. Shi, W. Zheng, L. Liang, Y. Yan, Y. Li, Astronomical and glacial forcing of East Asian summer monsoon variability. *Quat. Sci. Rev.* **115**, 132–142 (2015).
31. M. Bender, T. Sowers, L. Labeyrie, The Dole Effect and its variations during the last 130,000 years as measured in the Vostok ice core. *Global Biogeochem. Cycles* **8**, 363–376 (1994).
32. B. Malaizé, D. Paillard, J. Jouzel, D. Raynaud, The Dole effect over the last two glacial-interglacial cycles. *J. Geophys. Res. Atmos.* **104**, 14199–14208 (1999).
33. P. deMenocal, J. Ortiz, T. Guilderson, J. Adkins, M. Sarnthein, L. Baker, M. Yarusinsky, Abrupt onset and termination of the African Humid Period:: rapid climate responses to gradual insolation forcing. *Quat. Sci. Rev.* **19**, 347–361 (2000).
34. J. A. Collins, A. Govin, S. Mulitza, D. Heslop, M. Zabel, J. Hartmann, U. Röhl, G. Wefer, Abrupt shifts of the Sahara-Sahel boundary during Heinrich stadials. *Clim. Past* **9**, 1181–1191 (2013).
35. K. E. Kohfeld, S. P. Harrison, DIRTMAP: The geological record of dust. *Earth Sci. Rev.* **54**, 81–114 (2001).
36. G. Winckler, R. F. Anderson, M. Q. Fleisher, D. McGee, N. Mahowald, Covariant glacial-interglacial dust fluxes in the equatorial Pacific and Antarctica. *Science* **320**, 93–96 (2008).
37. D. McGee, W. S. Broecker, G. Winckler, Gustiness: The driver of glacial dustiness? *Quat. Sci. Rev.* **29**, 2340–2350 (2010).
38. V. Kolla, P. E. Biscaye, A. F. Hanley, Distribution of quartz in late Quaternary Atlantic sediments in relation to climate. *Quat. Res.* **11**, 261–277 (1979).
39. C. Skonieczny, P. Paillou, A. Bory, G. Bayon, L. Biscara, X. Crosta, F. Eynaud, B. Malaizé, M. Revel, N. Aleman, J. P. Barusseau, R. Vernet, S. Lopez, F. Grousset, African humid periods triggered the reactivation of a large river system in Western Sahara. *Nat. Commun.* **6**, 8751 (2015).
40. R. B. Wynn, P. P. E. Weaver, D. G. Masson, D. A. V. Stow, Turbidite depositional architecture across three interconnected deep-water basins on the north-west African margin. *Sedimentology* **49**, 669–695 (2002).
41. R. B. Husar, M. Prospero, L. L. Stowe, Characterization of tropospheric aerosols over the oceans with the NOAA advanced very high resolution radiometer optical thickness operational product. *J. Geophys. Res.* **102**, 16889–16909 (1997).
42. G. M. Henderson, R. F. Anderson, The U-series Toolbox for Paleoceanography. *Rev. Mineral. Geochem.* **52**, 493–531 (2003).
43. R. Francois, M. Frank, M. Rutgers van der Loeff, M. P. Bacon, W. Geibert Stephanie Kienast, R. F. Anderson, L. Bradtmiller, Z. Chase, G. Henderson Franco Marcantonio, S. E. Allen, Comment on "Do geochemical estimates of sediment focusing pass the sediment test in the equatorial Pacific?" by M. Lyle et al. *Paleoceanogr. Paleoclimatol.* **22**, PA1216 (2007).
44. A. N. Meckler, D. M. Sigman, K. A. Gibson, R. François, A. Martínez-García, S. L. Jaccard, U. Röhl, L. C. Peterson, R. Tiedemann, G. H. Haug, Deglacial pulses of deep-ocean silicate into the subtropical North Atlantic Ocean. *Nature* **495**, 495–498 (2013).
45. R. L. Edwards, J. H. Chen, G. J. Wasserburg, ^{238}U-^{234}U-^{230}Th-^{232}Th systematics and the precise measurement of time over the past 500, 000 years. *Earth Planet. Sci. Lett.* **81**, 175–192 (1987).
46. D. Paillard, L. Labeyrie, P. Yiou, AnalySeries 1.0: A Macintosh software for the analysis of geographical time-series. *Eos* **77**, 379 (1996).
47. R. B. Blackman, J. W. Tukey, *The Measurement of Power Spectra from the Point of View of Communication Engineering* (Dover Publications, 1958).
48. O. Bringham, *The Fast Fourier Transform* (Prentice Hall, 1974).
49. G. M. Jenkins, D. G. Watts, *Spectral Analysis and Its Applications* (Holden-Day, 1968).
50. K. M. R. Matsuzaki, F. Eynaud, B. Malaizé, F. E. Grousset, A. Tisserand, L. Rossignol, K. Charlier, E. Jullien, Paleoceanography of the Mauritanian margin during the last two climatic cycles: From planktonic foraminifera to African climate dynamics. *Mar. Micropaleontol.* **79**, 67–79 (2011).
51. P. J. Reimer, E. Bard, A. Bayliss, J. W. Beck, P. G. Blackwell, C. B. Ramsey, C. E. Buck, H. Cheng, R. L. Edwards, M. Friedrich, P. M. Grootes, T. P. Guilderson, H. Haflidason, I. Hajdas, C. Hatté, T. J. Heaton, D. L. Hoffmann, A. G. Hogg, K. A. Hughen, K. F. Kaiser, B. Kromer, S. W. Manning, M. Niu, R. W. Reimer, D. A. Richards, E. M. Scott, J. R. Southon, R. A. Staff, C. S. M. Turney, J. van der Plicht, IntCal13 and Marine13 radiocarbon age calibration curves 0–50,000 years cal BP. *Radiocarbon* **55**, 1869–1887 (2013).
52. L. E. Lisiecki, M. E. Raymo, A Pliocene–Pleistocene stack of 57 globally distributed benthic δ^{18}O records. *Paleoceanogr. Paleoclimatol.* 20, PA1003 (2005).
53. B. Martrat, J. O. Grimalt, N. J. Shackleton, L. de Abreu, M. A. Hutterli, T. F. Stocker, Four climate cycles of recurring deep and surface water destabilizations on the Iberian margin. *Science* **317**, 502–507 (2007).
54. W. B. Curry, G. P. Lohmann, Carbon deposition rates and deep water residence time in the equatorial Atlantic Ocean throughout the last 160,000 years, in *The Carbon Cycle and Atmospheric CO2: Natural Variations Archean to Present*, E. T. Sundquist, W. S. Broecker, Eds. (American Geophysical Union, 1985), vol. 32, pp. 285–301.
55. D. McGee, F. Marcantonio, J. F. McManus, G. Winckler, The response of excess ^{230}Th and extraterrestrial ^{3}He to sediment redistribution at the Blake Ridge, western North Atlantic. *Earth Planet. Sci. Lett.* **299**, 138–149 (2010).
56. J. Thomson, D. R. H. Green, P. Van Calsteren, T. O. Richter, T. C. E. Van Weering, Holocene sediment deposition on a NE Atlantic transect including Feni Drift quantified by radiocarbon and ^{230}Th$_{excess}$ methods. *Earth Planet. Sci. Lett.* **242**, 170–185 (2006).
57. J. Thomson, S. Colley, R. Anderson, G. T. Cook, A. B. MacKenzie, D. D. Harkness, Holocene sediment fluxes in the northeast Atlantic from ^{230}Th$_{excess}$ and radiocarbon measurements. *Paleoceanogr. Paleoclimatol.* **8**, 631–650 (1993).

58. F. Marcantonio, M. Lyle, R. Ibrahim, Particle sorting during sediment redistribution processes and the effect on ^{230}Th-normalized mass accumulation rates. *Geophys. Res. Lett.* **41**, 5547–5554 (2014).
59. D. McGee, G. Winckler, A. Borunda, S. Serno, R. F. Anderson, C. Recasens, A. Bory, D. Gaiero, S. L. Jaccard, M. Kaplan, J. F. McManus, M. Revel, Y. Sun, Tracking eolian dust with helium and thorium: Impacts of grain size and provenance. *Geochim. Cosmochim. Acta* **175**, 47–67 (2016).
60. G. M. Henderson, C. Heinze, R. F. Anderson, A. M. E. Winguth, Global distribution of the ^{230}Th flux to ocean sediments constrained by GCM modelling. *Deep Sea Res. Part I Oceanogr. Res. Pap.* **46**, 1861–1893 (1999).
61. C. T. Hayes, R. F. Anderson, M. Q. Fleisher, K.-F. Huang, L. F. Robinson, Y. Lu, H. Cheng, R. L. Edwards, S. B. Moran, ^{230}Th and ^{231}Pa on GEOTRACES GA03, the U.S. GEOTRACES North Atlantic transect, and implications for modern and paleoceanographic chemical fluxes. *Deep Sea Res. Part II Top. Stud. Oceanogr.* **116**, 29–41 (2014).
62. R. F. Anderson, M. Q. Fleisher, Y. Lao, Glacial–interglacial variability in the delivery of dust to the central equatorial Pacific Ocean. *Earth Planet. Sci. Lett.* **242**, 406–414 (2006).
63. W. Ehrmann, M. Seidel, G. Schmiedl, Dynamics of late quaternary north african humid periods documented in the clay mineral record of central aegean sea sediments. *Glob. Planet. Change* **107**, 186–195 (2013).
64. O. Crouvi, K. Schepanski, R. Amit, A. R. Gillespie, Y. Enzel, Multiple dust sources in the Sahara Desert: The importance of sand dunes. *Geophys. Res. Lett.* **39**, L13401 (2012).
65. S. Egerer, M. Claussen, C. Reick, T. Stanelle, The link between marine sediment records and changes in Holocene Saharan landscape: Simulating the dust cycle. *Clim. Past* **12**, 1009–1027 (2016).
66. S. Albani, M. N. Mahowald, G. Winckler, R. F. Anderson, L. I. Bradtmiller, B. Delmonte, R. François, M. Goman, N. G. Heavens, P. P. Hesse, S. A. Hovan, S. Kang, K. E. Kohfeld, H. Lu, V. Maggi, J. A. Mason, P. A. Mayewski, D. McGee, X. Miao, B. L. Otto-Bliesner, A. T. Perry, A. Pourmand, H. M. Roberts, N. Rosenbloom, T. Stevens, J. Sun, Twelve thousand years of dust: The Holocene global dust cycle constrained by natural archives. *Clim. Past* **11**, 869–903 (2015).
67. S. Albani, N. M. Mahowald, L. N. Murphy, R. Raiswell, J. K. Moore, R. F. Anderson, D. McGee, L. I. Bradtmiller, B. Delmonte, P. P. Hesse, P. A. Mayewski, Paleodust variability since the Last Glacial Maximum and implications for iron inputs to the ocean. *Geophys. Res. Lett.* 3944–3954 (2016).
68. O. M. Doherty, N. Riemer, S. Hameed, Control of Saharan mineral dust transport to Barbados in winter by the Intertropical Convergence Zone over West Africa. *J. Geophys. Res. Atmos.* **117**, D1911 (2012).
69. D. A. Ridley, C. L. Heald, J. M. Prospero, What controls the recent changes in African mineral dust aerosol across the Atlantic? *Atmos. Chem. Phys.* **14**, 5735–5747 (2014).
70. C. Skonieczny, A. Bory, V. Bout-Roumazeilles, W. Abouchami, S. J. G. Galer, X. Crosta, J. B. Stuut, I. Meyer, I. Chiapello, T. Podvin, B. Chatenet, A. Diallo, T. Ndiaye, The 7–13 March 2006 major Saharan outbreak: Multiproxy characterization of mineral dust deposited on the West African margin. *J. Geophys. Res. Atmos.* **116**, D18210 (2011).
71. C. Skonieczny, A. Bory, V. Bout-Roumazeilles, W. Abouchami, S. J. G. Galer, X. Crosta, A. Diallo, T. Ndiaye, A three-year time series of mineral dust deposits on the West African margin: Sedimentological and geochemical signatures and implications for interpretation of marine paleo-dust records. *Earth Planet. Sci. Lett.* **364**, 145–156 (2013).
72. D. McGee, E. Moreno-Chamarro, B. Green, J. Marshall, E. Galbraith, L. Bradtmiller, Hemispherically asymmetric trade wind changes as signatures of past ITCZ shifts. *Quat. Sci. Rev.* **180**, 214–228 (2018).
73. J. S. Singarayer, P. J. Valdes, W. H. G. Roberts, Ocean dominated expansion and contraction of the late Quaternary tropical rainbelt. *Sci. Rep.* **7**, 9382 (2017).

Acknowledgments: IMAGES core MD03-2705 was recovered by the *R/V Marion Dufresne* (Institut Paul Emile Victor) in 2003. C.S. is grateful to I. Tal and B. Hardt for laboratory assistance at MIT. This manuscript benefitted from comments by R. F. Anderson and three anonymous reviewers. The data visualization in Fig. 1 was produced with the Giovanni online data system, developed and maintained by NASA GES DISC. **Funding:** NSF Award OCE-1502985/1502925 to D.M., G.W., and P.J.P. C.S. was supported by the French national program LEFE/INSU. **Author contributions:** C.S. and D.M. designed the study. C.S. performed the isotopic analysis with the help of C.W.K. C.S. and D.M. interpreted results and wrote the manuscript. G.W. and A.B. discussed interpretation of results. L.I.B. performed carbonate measurements. R.D.P.-H. performed radiocarbon dating. L.R. helped in the picking of foraminifera for radiocarbon dating. B.M. helped in sampling the core. All authors contributed to the editing of the manuscript. **Competing interests:** The authors declare that they have no competing interest. **Data and materials availability:** All data needed to evaluate the conclusions in the paper are present in the paper and/or the Supplementary Materials. Additional data related to this paper may be requested from the authors.

Submitted 22 August 2018
Accepted 21 November 2018
Published 2 January 2019
10.1126/sciadv.aav1887

Citation: C. Skonieczny, D. McGee, G. Winckler, A. Bory, L. I. Bradtmiller, C. W. Kinsley, P. J. Polissar, R. De Pol-Holz, L. Rossignol, B. Malaizé, Monsoon-driven Saharan dust variability over the past 240,000 years. *Sci. Adv.* **5**, eaav1887 (2019).